Comparison of Crystal Structure and Theory for 2-Amino-1-methyl-6-phenylimidazo[4,5-*b*]pyridine

Sean Parkin,[†] Glenn A. Marsch,[†] Håkon Hope,[‡] Erin Whitney,[§] Nick W. Winter,[†] Michael E. Colvin,[||] James S. Felton,[†] and Kenneth W. Turteltaub*,[†]

Molecular and Structural Biology Division, Biology and Biotechnology Research Program, Lawrence Livermore National Laboratory, Livermore, California 94550, Department of Chemistry, University of California, Davis, California 95616, Williams College, Williams, Massachusetts 01267, and Sandia National Laboratory, Livermore, California 94551

Received October 2, 1995[⊗]

The crystal structure of the food mutagen 2-amino-1-methyl-6-phenylimidazo[4,5-*b*] pyridine (PhIP) has been determined by single-crystal X-ray crystallography. Crystals grown by evaporation of an aqueous solution form in the monoclinic space group $P2_1/n$ with two molecules of PhIP per asymmetric unit, along with six water molecules. The phenyl groups of these two PhIP molecules have torsion angles of different magnitude with respect to the plane of the imidazopyridine moiety. To maintain centrosymmetry, the crystal also contains an oppositely torsioned symmetry equivalent of each. The amino groups of both PhIP molecules take part in an extensive hydrogen bond network with the water of crystallization, forming long channels through the crystals parallel to the crystallographic *b* axis. The diffraction results are compared to theoretical calculations of the optimized geometry for a single PhIP molecule in vacuo as well as with water hydrogen-bonded to the exocyclic amine. In general, the agreement between the X-ray crystal structure of PhIP and its theory-derived counterpart in vacuo is within the combined experimental−theoretical uncertainty. The C−N bond to the exocyclic amine and the neighboring C═N imidazole bond are exceptions. This is attributed to the combined neglect of the crystal environment, waters of hydration, and the lack of coplanarity between the imidazole ring and the amine group in the calculations. To address the effect of waters of hydration, additional calculations were performed to optimize the geometry of a PhIP molecule with two water molecules hydrogen-bonded to the exocyclic amine. The resulting C−N exocyclic amine and C═N imidazole bond lengths were closer to those obtained by X-ray diffraction. The accord between theory and experiment demonstrates the utility of applying theory to (1) accurately predict structures of PhIP metabolites and intermediates that are too labile for study by conventional structural techniques such as X-ray crystallography and (2) assist in studying the mechanisms by which PhIP and its metabolites interact with proteins and DNA.

Introduction

The aminoimidazoazaarenes (AIAs)[1] comprise a class of heterocyclic amine mutagens formed in muscle meats cooked at high temperatures (*1*−*3*). These compounds are also found in smaller quantities in cigarette smoke (*4*), beer and wine (*5*), and some grain products (*6*). Formation of the compounds occurs by a pyrolytically-induced condensation of amino acids and creatine or creatinine during combustion or heating (*7*, *8*). Of the many species of AIAs detected in cooked meat, the most abundant is usually 2-amino-1-methyl-6-phenylimidazo-[4,5-*b*]pyridine (PhIP) (*1*, *9*), which is found at levels of up to 480 ppb.

PhIP (Figure 1) is a genotoxin that is moderately mutagenic in the Ames/*Salmonella* assay, inducing up to 2000 revertants/μg of mutagen (*2*, *10*, *11*). In addition, it is a potent rodent tumorigen, inducing lymphomas in mice (*12*, *13*) and colon and breast tumors in rats (*12*, *14*). The prevalence of PhIP in the western diet, coupled with its carcinogenicity in rodents, suggests that it may be relevant in the etiology of human cancer, particularly of the breast and colon.

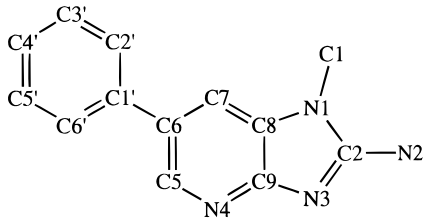

Figure 1. Structure of the heterocyclic amine food mutagen PhIP.

Like many bulky, aromatic carcinogens (*15*, *16*), PhIP is a stable nonreactive compound that is activated in vivo to highly reactive electrophilic intermediates. Cytochrome P450 monooxygenases oxidize PhIP to the N^2-hydroxy-PhIP (*N*-OH-PhIP) intermediate (*17*−19) which acts as a substrate for cellular acetyl- and sulfonyltransferases to form N^2-acetoxy-PhIP and N^2-sulfonyl-PhIP, respectively (*20*−*22*). Covalent binding of these electrophilic esters to the C8 atom of guanine is facile both in vitro and in vivo, resulting primarily in an N^2-(2′-deoxyguanosin-8-yl)-PhIP adduct (*23*−*25*), but other adducts may also exist (*24*−*26*).

* To whom correspondence should be addressed.
[†] Lawrence Livermore National Laboratory.
[‡] University of California.
[§] Williams College.
[||] Sandia National Laboratory.
[⊗] Abstract published in *Advance ACS Abstracts,* February 15, 1996.
[1] Abbreviations: aminoimidazoazaarene, AIA; 2-amino-1-methyl-6-phenylimidazo[4,5-*b*]pyridine, PhIP; Hartree−Fock, HF.

0893-228x/96/2709-0574$12.00/0

The noncovalent interaction of PhIP with DNA occurs within a millisecond time scale *via* a groove-binding mechanism (*27*). Decomposition of N^2-acetoxy-PhIP, or its covalent addition to guanine bases, occurs rapidly (*21*, *25*) with a half-life of ~2 min in aqueous buffers at 25 °C (*26*). Thus, the covalent addition stage is likely preceded by the initial noncovalent groove-binding interaction of the PhIP metabolite to DNA. The groove-binding mechanism was interpreted as resulting from PhIP's small size combined with the nonplanarity of the phenyl ring with respect to the imidazopyridine ring system (*27*). Conformational modeling using potential energy minimization searches suggests that, upon covalent interaction with DNA, this phenyl ring dihedral angle may decrease from 45° to *ca*. 21° (*28*).

Prior to this work, no experimentally derived three-dimensional structures of PhIP had been obtained. We present here the X-ray crystal structure of PhIP and compare it to that derived from quantum mechanical calculations. The aims in doing so were to computationally generate realistic structures of PhIP and related species too labile for crystallographic study (e.g., acetoxy and sulfate esters of PhIP) which could then be used in mechanistic or structural studies of PhIP interactions with DNA and proteins.

Experimental Procedures

Chemicals. **Caution:** *The heterocyclic aromatic amine PhIP is carcinogenic in rodents and should be handled carefully according to appropriate Environmental Health and Safety protocols*. PhIP was purchased from Toronto Research Chemicals (Downsview, Ontario, Canada) and was used without further purification.

X-Ray Crystallography. Crystals were grown by the slow evaporation of an aqueous solution, which produced a large number of extremely thin, fragile needles. After several months, a few small blocky crystals were also observed. Initial investigation of the needle-form crystals revealed a monoclinic cell, with approximate dimensions $a = 11.18$ Å, $b = 7.23$ Å, $c = 35.51$ Å, $\beta = 99.16°$, but the space group was indeterminate. These crystals had a tendency to splinter lengthwise and to crack perpendicular to the needle axis. They all gave wide, multiply peaked ω-scans. Further investigation of these needles was abandoned in favor of the small blocky modification.

A roughly cubic crystal of approximate dimension 0.1 mm was mounted on a Syntex $P2_1$ diffractometer into the (initially deflected) cold-stream path of a modified Syntex LT-1 low-temperature apparatus at 130 K. The diffraction quality of these crystals was poor (but much better than the needle form), with typical ω-scan base-to-base widths of ~1°. The crystal indexed as monoclinic, $P2_1/n$ with $a = 11.156(4)$, $b = 7.219(3)$, $c = 35.552(14)$, $\beta = 98.88(3)°$, essentially the same as the needle form. The origin of the difference in crystal morphology remains unknown. The blocky crystals, however, were only observed long after the growth of needle-shaped crystals had ceased.

Diffraction data were collected at 130 K with Cu Kα (λ = 1.54178 Å) radiation from a sealed tube source. The structure was solved by direct methods (*29*) and refined by weighted full-matrix least-squares minimization on F^2 with SHELXL-93 (*30*). In the least-squares refinement, both phenyl rings were constrained to be identical, flat and to obey mm2 (C_{2v}) symmetry; i.e., equivalent bonds and angles in each were tied to the same (refined) variable. The aminomethylimidazopyridine moieties, however, were loosely restrained to similar geometries. All hydrogen atoms belonging to the main molecules were found in difference electron density maps and were refined using a riding model ($d_{C\text{-}H} = 0.98$ Å, $d_{N\text{-}H} = 0.94$ Å). Difference map evidence was found for 10 of the 12 possible hydrogens attached to the water molecules, and all were in positions that formed plausible hydrogen bonds. They were fixed at 0.85 Å from their respective oxygen atoms. The torsion angles of the phenyl groups relative to the imidazopyridine moieties refined freely. An absorption correction (*31*) was applied, and refinement converged with a conventional R factor (on F for data with $I > 2\sigma(I)$) of 7.58%. The final difference map was featureless, the largest peak being 0.29 e Å^{-3}. Data collection and refinement statistics are given in Table 1.

Table 1. Crystal and Structure Refinement Data

identification code	PhIP
empirical formula	$C_{26}H_{36}N_8O_6$
formula wt	500.59
temp (K)	130(1)
wavelength (Å)	1.54178
cryst system	monoclinic
unit cell dimensions	
a (Å)	11.156(4)
b (Å)	7.219(3)
c (Å)	35.552(14)
α (deg)	90
β (deg)	98.88(3)
γ (deg)	90
volume (Å^3)	2829(2)
Z	4
density (calcd)	1.175 Mg m^{-3}
absorption coeff (mm^{-1})	0.690
F(000)	1072
cryst size (mm)	0.1 × 0.1 × 0.1
θ range for data collection (deg)	4.01−54.06
index ranges	$-11 \le h \le 11$, $0 \le k \le 7$, $0 \le l \le 37$
reflections collected	3433 (unique set)
independent reflections	3433 (R_{int} undefined)
absorption correction	XABS2 (*31*)
max and min transmission	0.93 and 0.89
refinement method	full-matrix least-squares on F^2
data/restraints/parameters	3433/92/391
goodness-of-fit on F^2	1.092
final R indices [$I > 2\sigma(I)$]	$R_1 = 0.0758$
R indices (all data)	$R_1 = 0.1125$
extinction coeff	0.00019(14)
largest diff peak and hole (e·Å^{-3})	0.29 and −0.32

Quantum Mechanical Calculations. The geometry of the isolated PhIP molecule in vacuo was optimized at the Hartree−Fock (HF) level of theory using a standard 6-31G* basis set (*32*). All 118 electrons were explicitly included in the calculations and were described by the 59 doubly occupied molecular orbitals of the ground state of the PhIP molecule. Additional calculations were carried out to assess the effects of solvation, basis set size, and the planarity of the exocyclic amine group on the PhIP structure. For these calculations, waters of crystallization were modeled by adding two water molecules to the PhIP calculations constrained to be 1.82 Å from the exocyclic amine hydrogens, but otherwise fully optimized.

HF 6-31G* calculations for organic molecules (*33*) have shown that predicted C−H, N−H, and O−H bond lengths are usually underestimated by ~0.01 Å. Single bonds between non-hydrogen atoms are calculated with comparable accuracy, but double bonds tend to be underestimated by ~0.02 Å. Calculations that include electron correlation predict longer bond lengths, in better agreement with experiment. Similar comparisons to experiment for $-NH_2$, $-CH_2$, and $-OH_2$ bond angles indicate that angles are overestimated by 1−2° (*33*) depending on which heavy atom is involved and the nature of its bonding to the remainder of the molecule. Reoptimization of the PhIP geometry with a 6-31G** basis set, which includes *2*p -type functions on the hydrogens, changed the bond lengths by only ~0.001 Å and bond angles by 0.1°.

Results and Discussion

For consistency, we have retained the general form of the atom numbering scheme used in earlier work, but with "A" and "B" appended to distinguish the two crystallographically inequivalent PhIP molecules (Figure

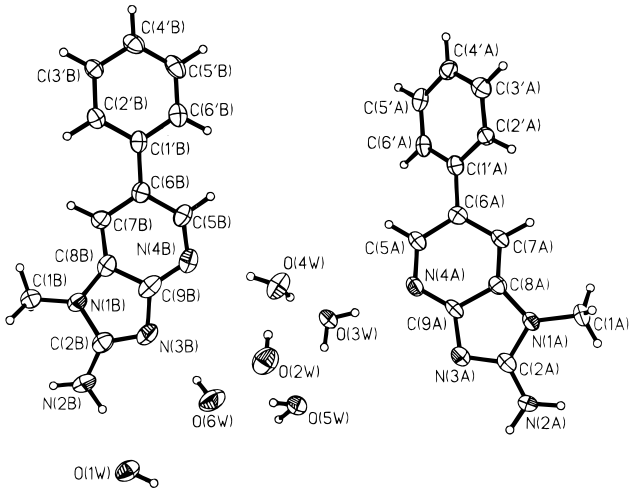

Figure 2. The two crystallographically inequivalent PhIP molecules and six waters of crystallization.

Table 2. Atomic Coordinates ($\times 10^4$) and Equivalent Isotropic Thermal Parameters ($Å^2 \times 10^3$) for PhIP[a]

atom	x[a]	y[a]	z[a]	U_{eq}[a,b]
N(1A)	6459(4)	3872(6)	−761(1)	30(1)
C(1A)	7729(4)	3649(9)	−794(2)	39(2)
C(2A)	5958(5)	4077(8)	−432(2)	34(1)
N(2A)	6614(4)	4049(7)	−88(1)	40(1)
N(3A)	4751(4)	4344(7)	−501(1)	36(1)
N(4A)	3348(4)	4437(6)	−1090(1)	33(1)
C(5A)	3270(5)	4262(8)	−1468(2)	31(1)
C(6A)	4251(4)	3936(7)	−1665(1)	28(1)
C(7A)	5423(4)	3824(7)	−1450(2)	29(1)
C(8A)	5504(4)	3996(8)	−1068(2)	28(1)
C(9A)	4453(4)	4283(8)	−890(2)	29(1)
C(1′A)	4034(3)	3770(7)	−2082(1)	28(1)
C(2′A)	4863(3)	4469(7)	−2304(1)	28(1)
C(3′A)	4616(4)	4406(7)	−2698(1)	33(1)
C(4′A)	3569(3)	3591(7)	−2880(1)	33(1)
C(5′A)	2754(4)	2859(7)	−2667(1)	34(2)
C(6′A)	2979(4)	2936(7)	−2272(1)	32(2)
N(1B)	−4994(4)	9150(6)	−1133(1)	33(1)
C(1B)	−6299(5)	9417(9)	−1181(2)	39(2)
C(2B)	−4208(5)	8996(8)	−792(2)	36(2)
N(2B)	−4587(4)	9198(7)	−461(1)	45(1)
N(3B)	−3065(4)	8612(7)	−841(1)	39(1)
N(4B)	−2186(4)	8178(7)	−1423(2)	41(1)
C(5B)	−2453(5)	8182(8)	−1801(2)	36(2)
C(6B)	−3592(5)	8542(7)	−2012(2)	31(1)
C(7B)	−4563(5)	8922(7)	−1810(2)	30(1)
C(8B)	−4306(5)	8874(7)	−1422(2)	31(1)
C(9B)	−3119(5)	8534(8)	−1230(2)	38(2)
C(1′B)	−3768(4)	8574(6)	−2433(1)	31(1)
C(2′B)	−4710(4)	9599(7)	−2641(1)	31(1)
C(3′B)	−4860(4)	9655(7)	−3036(1)	29(1)
C(4′B)	−4091(4)	8689(7)	−3232(1)	36(2)
C(5′B)	−3151(4)	7689(7)	−3033(1)	40(2)
C(6′B)	−2981(4)	7632(7)	−2638(1)	35(2)
O(1W)	−3251(4)	8804(6)	298(1)	44(1)
O(2W)	844(4)	11008(6)	−655(1)	52(1)
O(3W)	1079(3)	4699(6)	−849(1)	40(1)
O(4W)	368(4)	8199(6)	−1187(1)	51(1)
O(5W)	733(3)	6216(6)	−160(1)	44(1)
O(6W)	−949(4)	9112(7)	−296(1)	60(1)

[a] Numbers in parentheses are estimated standard deviations derived from the least-squares variance−covariance matrices. [b] U_{eq} is defined as one-third of the trace of the orthogonalized U_{ij} tensor.

2); atomic coordinates are given in Table 2. Bond length and angle differences between the two PhIP molecules were insignificant; the root-mean-square (rms) deviations were 0.008 Å and 0.56°, respectively. Only three of the bond lengths and four of the bond angles differed by more than the sum of their respective estimated standard deviations (esds). All were well within the accuracy limit for first-row atom structures imposed by the spherical atom scattering factor approximation (*34*). In the following section, where bond lengths and angles are given as the average over the two crystallographically inequivalent PhIP molecules, the "A" and "B" suffixes are dropped. Geometric data for both experimental and theoretical models are given in Tables 3 and 4.

In general, differences between experimental and theoretical bond lengths are consistent with expected errors at the HF 6-31G* level of calculation and are within combined experimental−theoretical uncertainty,

Table 3. Bond Lengths (Å) for PhIP Molecules A and B Compared to Theory

atoms	PhIP A[a] (X-ray)	PhIP B[a] (X-ray)	average[a] (X-ray)	theory[b] (isolated)	theory[b] (solvated)
N1−C2	1.380(6)	1.387(7)	1.384(5)	1.36_4	1.36_2
N1−C8	1.405(6)	1.391(7)	1.398(5)	1.38_9	1.38_6
N1−C1	1.448(6)	1.452(6)	1.450(4)	1.44_4	1.44_3
C2−N2	1.325(7)	1.319(7)	1.322(5)	1.37_4	1.35_7
C2−N3	1.345(6)	1.343(7)	1.344(5)	1.28_8	1.30_4
N3−C9	1.372(6)	1.376(7)	1.374(5)	1.37_6	1.37_2
N4−C9	1.329(6)	1.330(7)	1.330(5)	1.31_3	1.31_2
N4−C5	1.341(6)	1.356(7)	1.349(5)	1.32_1	1.32_5
C5−C6	1.405(7)	1.398(7)	1.402(5)	1.39_7	1.39_3
C6−C7	1.411(7)	1.417(7)	1.414(5)	1.39_6	1.40_0
C6−C1′	1.470(6)	1.479(7)	1.475(5)	1.48_9	1.48_8
C7−C8	1.352(7)	1.363(7)	1.357(5)	1.37_1	1.36_8
C8−C9	1.432(7)	1.415(7)	1.424(5)	1.40_1	1.40_5
C1′−C6′	1.400(3)	1.400(3)	1.400(2)	1.39_3	1.39_3
C1′−C2′	1.400(3)	1.400(3)	1.400(2)	1.39_3	1.39_3
C2′−C3′	1.388(4)	1.388(4)	1.388(3)	1.38_4	1.38_4
C3′−C4′	1.376(4)	1.376(4)	1.376(3)	1.38_5	1.38_5
C4′−C5′	1.376(4)	1.376(4)	1.376(3)	1.38_5	1.38_5
C5′−C6′	1.388(4)	1.388(4)	1.388(3)	1.38_5	1.38_5

[a] Numbers in parentheses are estimated standard deviations derived from the least-squares variane−covariance matrix. [b] Subscripts denote reduced precision in the last decimal place.

Table 4. Bond and Selected Torsion Angles (deg) for PhIP Molecules A and B Compared to Theory

atoms	molecule A[a]	molecule B[a]	average[a]	theory (isolated)	theory (solvated)
C2−N1−C8	107.0(4)	106.8(4)	106.9(3)	105.2	105.8
C2−N1−C1	127.6(4)	127.0(5)	127.3(3)	127.7	127.1
C8−N1−C1	125.3(4)	126.1(4)	125.7(3)	126.9	126.9
N2−C2−N3	124.4(5)	125.5(5)	125.0(4)	124.3	123.4
N2−C2−N1	122.8(5)	121.7(5)	122.3(4)	120.7	122.6
N3−C2−N1	112.8(5)	112.8(5)	112.8(4)	115.0	114.0
C2−N3−C9	104.9(4)	104.2(4)	104.6(3)	104.7	105.1
C9−N4−C5	116.1(4)	116.2(5)	116.2(3)	116.2	116.2
N4−C5−C6	125.4(5)	125.9(5)	125.7(4)	125.4	125.4
C5−C6−C7	117.9(5)	117.7(5)	117.8(4)	118.1	118.0
C5−C6−C1′	119.7(4)	121.0(5)	120.4(3)	120.8	121.0
C7−C6−C1′	122.4(4)	121.3(4)	121.9(3)	121.1	121.0
C8−C7−C6	116.8(5)	116.7(5)	116.8(4)	116.4	116.5
C7−C8−N1	134.3(5)	133.6(5)	134.0(4)	134.1	134.1
C7−C8−C9	121.7(5)	121.9(5)	121.8(4)	120.8	120.7
N1−C8−C9	103.9(4)	104.5(5)	104.2(3)	105.2	105.2
N4−C9−N3	126.6(4)	126.7(5)	126.7(3)	126.7	126.9
N4−C9−C8	122.0(5)	121.5(5)	121.8(4)	123.2	123.2
N3−C9−C8	111.4(4)	111.8(5)	111.6(3)	110.0	110.0
C6′−C1′−C2′	117.6(4)	117.6(4)	117.6(3)	118.2	118.1
C6′−C1′−C6	121.2(3)	121.5(3)	121.4(2)	120.9	121.4
C2′−C1′−C6	121.3(3)	120.9(3)	121.1(2)	120.9	120.8
C3′−C2′−C1′	120.8(3)	120.8(3)	120.8(2)	120.9	121.0
C4′−C3′−C2′	120.7(3)	120.7(3)	120.7(2)	120.2	120.3
C5′−C4′−C3′	119.4(4)	119.4(4)	119.4(3)	119.4	119.4
C4′−C5′−C6′	120.7(3)	120.7(3)	120.7(2)	120.3	120.3
C5′−C6′−C1′	120.8(3)	120.8(3)	120.8(2)	120.9	120.9
phenyl torsion	±36.0	±24.6		±45	±45

[a] Numbers in parentheses are estimated standard deviations derived from the least-squares variance−covariance matrix.

though bonds C2−N2 and C2−N3 are notable exceptions (Table 3). The rms deviation in bond lengths and angles between the isolated in vacuo theoretical model and the average of the experimental models was 0.022 Å for all bonds (0.014 Å excluding C2−N2 and C2−N3) and 0.88° for all angles. The phenyl rings are extremely similar, even down to the distortion from regular hexagonal planarity. Torsional angles of the phenyl rings relative to the pyridine−imidazo moiety, however, are different. The theoretical model gave an energy minimum for a torsion of 45° (Table 4). Owing to the symmetry of the molecule, an equivalent minimum also exists at −45°, as has been indicated by previous calculations (*27*). Indeed, statistically one would expect an equal population of phenyl groups twisted in opposite directions. This is borne out in the crystalline state, where each of the two crystallographically inequivalent PhIP molecules has an oppositely torsioned symmetry equivalent (PhIP A = ±36.0°, PhIP B = ±24.6°). The torsion angle differences between experimental and theoretical PhIP models can likely be accounted for in terms of crystal packing forces (*35*). It is interesting to note that the magnitude of these differences is similar to that predicted when PhIP covalently binds to DNA and orients itself in the major groove (*28*). The experimental and theoretical pyridine rings are also very similar, though bonds involving N4 are somewhat shorter in the computational results. This is possibly due to neglect of hydrogen bonding to water, but is consistent with the intrinsic errors in HF 6-31G* calculations discussed in the previous section. The pyridine−imidazole ring fusion between C8 and C9 is also shorter in the theoretical model. This may be related to 6-31G* underestimation of bond lengths and to the low delocalization of the imidazole π-electron system, which in turn may be due to the prediction of nonplanarity for the exocyclic amine group, as described below.

Experimental bond length evidence suggests that there is significant localization of charge between C2 and N2 and a correspondingly lower bond order between C2 and N3. Indeed, the amine hydrogen positions obtained from difference electron density maps were close to planar with the imidazole ring. The nonplanarity predicted by the theoretical model leads to substantially more double bond character between C2 and N3 and a longer C2−N2 amine bond with pyramidal geometry about the amine nitrogen. The degree of N pyramidalization is determined by the balance between the p-conjugation of the nitrogen lone pair with the aromatic system and the use of highly directional sp^3 orbitals for the amine bonding. The shorter C=N bond and longer C-NH_2 bond predicted by the HF calculations are consistent with the calculated pyramidalization. This may indicate that theory for a model in vacuo slightly underestimates the *p*-conjugation of the nitrogen lone pair as compared to the crystal environment. The largest differences between experimental and theoretical models are in bonds involving nitrogen atoms, and are probably related to neglect of the hydrogen bonding network observed in the crystal structure. Calculation of the optimum PhIP geometry was thus carried out including two waters constrained to the experimentally determined distance from the exocyclic amine nitrogen, but otherwise fully optimized. The rms deviation in bond lengths between experiment and this partially solvated PhIP model was reduced to 0.017 Å (0.013 Å for all bonds except C2−N2 and C2−N3). In particular, the results show a shortening of the amine C2−N2 bond from 1.37_4 to 1.35_7 Å and a slight

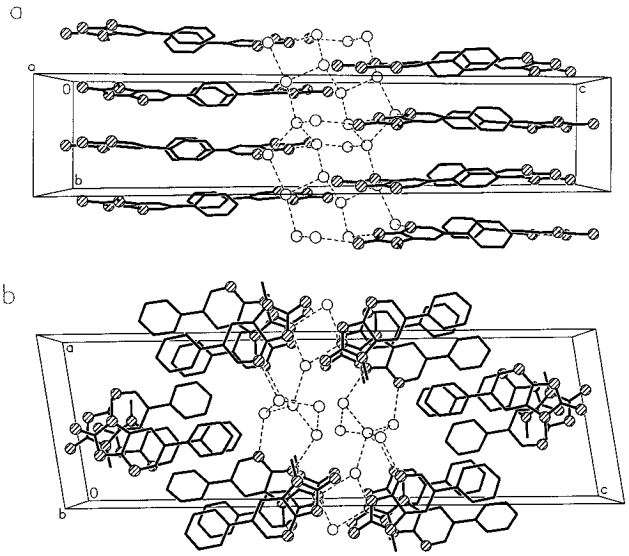

Figure 3. The PhIP crystal unit cell showing the channels of hydrogen-bonded water of crystallization. (a) View down the *a* axis. (b) View down the *b* axis.

lengthening of the C2−N3 double bond from 1.28_8 to 1.30_4 Å (subscripts denote reduced precision in the last decimal place). Rms bond angle deviations between this model and the experimental model also showed improvement over the isolated molecule model, from 0.88° to 0.77°. Inclusion of solvent increases the agreement with experiment so that the deviations for bonds C2−N2 and C2−N3 are decreased from 0.05_2 and 0.05_6 Å, respectively, against the in vacuo model to 0.03_5 and 0.04_0 Å, respectively, for the partially solvated model. These latter deviations are now on the borderline of the (estimated) combined experimental−theoretical uncertainty (about 0.03 to 0.04 Å). The planarity of the amine group with the imidazole was not significantly affected. Calculations with the amine and imidazole groups constrained to coplanarity showed increased delocalization of the N2−C2−N3 π-electron system and also improved the agreement with the experimental bond lengths. Further calculations with additional waters of hydration are underway.

In the crystal (Figures 2 and 3a,b), the two PhIP molecules and six waters are involved in an extensive hydrogen bonded network. The amine group of molecule A [atom N(2A)] is hydrogen bonded to equivalents of both water O(5W) and atom N(3A) of another PhIP molecule symmetrically related about the 2_1 screw axis. Atom N(2B) interacts with two waters, O(1W) in the same asymmetric unit and a glide equivalent O(1W). In addition to its H-bond to an equivalent of N(2A), atom N(3A) is also H-bonded to a (different) glide related O(1W) water, which bridges two (inequivalent) PhIP molecules. Atom N(3B), on the other hand, forms only one H-bond, to water O(6W) in the same asymmetric unit. Atoms N(4A) and N(4B) are both H-bonded in a trigonal planar fashion to only one atom each [O(3W) and O(4W), respectively], all within the same asymmetric unit. The six water molecules are situated about the 2_1 screw axis, forming long channels which run the length of the crystal parallel to the *b* axis. The H-bonding coordination is fourfold about all of these waters except O(4W), which is threefold. Water O(2W) is coordinated only to other water molecules.

It may be necessary to include the full crystalline environment of the PhIP molecule to achieve complete

agreement with the X-ray diffraction results. Although the hydrogen-bond network between PhIP and water found in these crystals is rather complex, the geometry about the nitrogen atoms themselves is quite straightforward. It can be modeled (at significant cost in terms of computing resources) simply by including appropriately constrained water molecules in the calculations.

Conclusions

Comparison of the crystal structure and theory permits the construction of theoretical models more realistic than the simple view of isolated molecules in vacuo. Although the hydrogen-bonding environment about each PhIP molecule is dynamic in vivo and static in the crystal structure, the structure of PhIP obtained from water solvated crystals is more likely than the theoretically-derived structure to be a realistic model of PhIP as it exists in vivo. The major reason for this is the effect of environment (especially hydrogen bonding) on molecular structure, electronic configuration, and hence on reactivity. After incorporating knowledge of the hydrogen-bonding network obtained from the PhIP crystal structure into ab initio calculations, the agreement between theory and experiment was enhanced dramatically. We anticipate corresponding improvements in theoretical models of PhIP metabolites if they are constructed in a similar fashion, i.e., by placing hydrogen-bonding waters at chemically intuitive positions and using the same 6-31G* basis sets used for our PhIP calculations. Such models should allow a more realistic view of how structure and steric effects influence the interaction of PhIP and metabolites with biological macromolecules, including DNA and proteins that metabolize PhIP (e.g., cytochrome P4501A2).

Acknowledgment. This work was performed in part under the auspices of the U.S. Department of Energy, Contract No. W-7405-ENG-48, at the Lawrence Livermore National Laboratory, and was partially supported by grants from the NIH (CA55861) and USAMRDC (MM#4559FLB).

References

(1) Felton, J. S., Knize, M. G., Shen, N. H., Andresen, B. D., Bjeldanes, L. F., and Hatch, F. T. (1986) Identification of the mutagens in cooked beef. *Environ. Health Perspect.* **67**, 17−24.

(2) Felton, J. S., and Knize, M. G. (1991) Occurrence, identification, and bacterial mutagenicity of heterocyclic amines in cooked food. *Mutat. Res.* **259**, 205−217.

(3) Zhang, X.-M., Wakabayashi, K., Liu, Z.-C., Sugimura, T., and Nagao, M. (1988) Mutagenic and carcinogenic heterocyclic amines in Chinese cooked foods. *Mutat. Res.* **201**, 181−188.

(4) Manabe, S., Tohyama, K., Wada, O., and Aramaki, T. (1991) Detection of a carcinogen, 2-amino-1-methyl-6-phenylimidazo[4,5-*b*]pyridine (PhIP), in cigarette smoke condensate. *Carcinogenesis* **12**, 1945−1947.

(5) Manabe, S., Suzuki, H., Wada, O., and Ueki, A. (1993) Detection of the carcinogen 2-amino-1-methyl-6-phenylimidazo[4,5-*b*]pyridine in beer and wine. *Carcinogenesis* **14**, 899−901.

(6) Knize, M. G., Cunningham, P. L., Griffin, E. A., Jr., Jones, A. L., and Felton, J. S. (1994) Characterization of mutagenic activity in cooked grain food products. *Food Chem. Toxicol.* **32**, 15−21.

(7) Skog, K., Knize, M. G., Felton, J. S., and Jagerstad, M. (1992) Formation of new heterocyclic amine mutagens by heating creatinine, alanine, threonine, and glucose. *Mutat. Res.* **268**, 191−197.

(8) Jagerstad, M., Skog, K., Grivas, S., and Olsson, K. (1991) Formation of heterocyclic amines using model systems. *Mutat. Res.* **259**, 219−233.

(9) Sinha, R., Rothman, N., Brown, E. D., Salmon, C. P., Knize, M. G., Swanson, C. A., Rossi, S. C., Mark, S. D., Levander, O. A., and Felton, J. S. (1995) High concentrations of the carcinogen 2-amino-1-methyl-6-phenylimidazo[4,5-*b*]pyridine (PhIP) can occur in chicken but are dependent on the cooking method. *Cancer Res.* **55**, 4516−4519.

(10) Felton, J. S., and Knize, M. G. (1990) Heterocyclic amine mutagens/carcinogens in foods. In *Handbook of Experimental Pharmacology* (Cooper, C. S., and Grover, P. L., Eds.) Vol. 94/I, pp 471−502, Springer-Verlag, Berlin and Heidelberg.

(11) Knize, M. G., and Felton, J. S. (1986) The synthesis of the cooked-beef mutagen 2-amino-1-methyl-6-phenylimidazo[4,5-*b*]pyridine and its 3-methyl isomer. *Heterocycles* **24**, 1815−1819.

(12) Wakabayashi, K., Nagao, M., Esumi, H., and Sugimura, T. (1992) Food-derived mutagens and carcinogens. *Cancer Res.* **52**, 2092s−2098s.

(13) Esumi, H., Ohgaki, H., Kohzen, E., Takayama, S., and Sugimura, T. (1989) Induction of lymphoma in CDF1 mice by the food mutagen, 2-amino-1-methyl-6-phenylimidazo[4,5-*b*]pyridine. *Jpn. J. Cancer Res.* **80**, 1176−1178.

(14) Ito, N., Hasegawa, R., Sano, M., Tamano, S., Esumi, H., Takayama, S., and Sugimura, T. (1991) A new colon and mammary carcinogen in cooked food, 2-amino-1-methyl-6-phenylimidazo[4,5-*b*]pyridine (PhIP). *Carcinogenesis* **12**, 1503−1506.

(15) Autrup, H. (1990) Carcinogen metabolism in cultured human tissues and cells. *Carcinogenesis* **11**, 707−712.

(16) Conney, A. H. (1982) Induction of microsomal enzymes by foreign chemicals and carcinogenesis by polycyclic aromatic compounds. *Cancer Res.* **42**, 4875−4917.

(17) Turteltaub, K. W., Knize, M. G., Buonarati, M. H., McManus, M. E., Veronese, M. E., Mazrimas, J. A., and Felton, J. S. (1990) Metabolism of 2-amino-1-methyl-6-phenylimidazo[4,5-*b*]pyridine (PhIP) by liver microsomes and isolated rabbit cytochrome P450 isozymes. *Carcinogenesis* **11**, 941−946.

(18) Holme, J. A., Wallin, H., Brunborg, G., Soderlund, E. J., Hongslo, J. K., and Alexander, J. (1989) Genotoxicity of the food mutagen 2-amino-1-methyl-6-phenylimidazo[4,5-*b*]pyridine (PhIP): formation of 2-hydroxyamino-PhIP, a direct-acting genotoxic metabolite. *Carcinogenesis* **10**, 1389−1396.

(19) Frandsen, H., Rasmussen, E. S., Nielsen, P. A., Farmer, P., Dragsted, L., and Larsen, J. C. (1991) Metabolic formation, synthesis and genotoxicity of the *N*-hydroxy derivative of the food mutagen 2-amino-1-methyl-6-phenylimidazo[4,5-*b*]pyridine (PhIP). *Mutagenesis* **6**, 93−98.

(20) Buonarati, M. H., Turteltaub, K. W., Shen, N. H., and Felton, J. S. (1990) Role of sulfation and acetylation in the activation of 2-hydroxyamino-1-methyl-6-phenylimidazo[4,5-*b*]pyridine to intermediates which bind DNA. *Mutat. Res.* **245**, 185−190.

(21) Kaderlik, K. R., Minchin, R. F., Mulder, G. J., Ilett, K. F., Daugaard-Jensen, M., Teitel, C. H., and Kadlubar, F. F. (1994) Metabolic activation pathway for the formation of DNA adducts of the carcinogen 2-amino-1-methyl-6-phenylimidazo[4,5-*b*]pyridine (PhIP) in rat extrahepatic tissues. *Carcinogenesis* **15**, 1703−1709.

(22) Turesky, R. J., Lang, N. P., Butler, M. A., Teitel, C. H., and Kadlubar, F. F. (1991) Metabolic activation of carcinogenic heterocyclic aromatic amines by human liver and colon. *Carcinogenesis* **12**, 1839−1845.

(23) Nagaoka, H., Wakabayashi, K., Kim, S.-B., Kim, I.-S., Tanaka, Y., Ochiai, M., Tada, A., Nukaya, H., Sugimura, T., and Nagao, M. (1992) Adduct formation at C-8 of guanine on *in vitro* reaction of the ultimate form of 2-amino-1-methyl-6-phenylimidazo[4,5-*b*]pyridine with 2′-deoxyguanosine and its phosphate esters. *Jpn. J. Cancer Res.* **83**, 1025−1029.

(24) Lin, D., Kaderlik, K. R., Turesky, R. J., Miller, D. W., Lay, J. O., Jr., and Kadlubar, F. F. (1992) Identification of *N*-(deoxyguanosin-8-yl)-2-amino-1-methyl-6-phenylimidazo[4,5-*b*]pyridine as the major adduct formed by the food-borne carcinogen, 2-amino-1-methyl-6-phenylimidazo[4,5-*b*]pyridine, with DNA. *Chem. Res. Toxicol.* **5**, 691−697.

(25) Frandsen, H., Grivas, S., Andersson, R., Dragsted, L., and Larsen, J. C. (1992) Reaction of the N^2-acetoxy derivative of 2-amino-1-methyl-6-phenylimidazo-[4,5-*b*]pyridine (PhIP) with 2′-deoxyguanosine and DNA. Synthesis and identification of N^2-(2′-deoxyguanosin-8-yl)-PhIP. *Carcinogenesis* **13**, 629−635.

(26) Marsch, G. A., Goldman, E. N., Fultz, E., Shen, N. H., and Turteltaub, K. W. (1995) Heterogeneous DNA adduct formation in vitro by the acetylated food mutagen 2-(acetoxyamino)-1-methyl-6-phenylimidazo[4,5-*b*]pyridine: a fluorescence spectroscopic study. *Chem. Res. Toxicol.* **8**, 659−670.

(27) Marsch, G. A., Ward, R. L., Colvin, M., and Turteltaub, K. W. (1994) Noncovalent DNA groove-binding by 2-amino-1-methyl-6-phenylimidazo[4,5-*b*]pyridine. *Nucleic Acids Res.* **22**, 5408−5415.

(28) Carothers, A. M., Yuan, W., Hingerty, B. E., Broyde, S., Grunberger, D., and Snyderwine, E. G. (1994) Mutation and repair induced by the carcinogen 2-(hydroxyamino)-1-methyl-6-phenylimidazo[4,5-*b*]pyridine (*N*-OH-PhIP) in the dihydrofolate reductase gene of Chinese hamster ovary cells and conformational modeling of the dG-C8-PhIP adduct in DNA. *Chem. Res. Toxicol.* **7**, 209−218.
(29) Sheldrick, G. M. (1990) 'TREF' in Siemens SHELXTL. An integrated system for solving, refining and displaying crystal structures from diffraction data, version 4.2. Siemens Analytical X-Ray Instruments, Madison, WI, USA.
(30) Sheldrick, G. M. (1993) SHELXL93 crystal structure refinement program. University of Göttingen, Germany.
(31) Parkin, S., Moezzi, B., and Hope, H. (1995) XABS2—An empirical absorption correction program. *J. Appl. Crystallogr.* **28**, 53−56.
(32) Hariharan, P. C., and Pople, J. A. (1973) The influence of polarization functions on molecular orbital hydrogenation energies. *Theor. Chim. Acta* **28**, 213−222.
(33) Johnson, B. G., Gill, P. M. W., and Pople, J. A. (1993) The performance of a family of density functional methods. *J. Chem. Phys.* **98**, 5612−5626.
(34) Coppens, P., Sabine, T. M., Delaplane, R. G., and Ibers, J. A. (1969) An experimental determination of the asphericity of the atomic charge distribution in oxalic acid dihydrate. *Acta Crystallogr.* B**25**, 2451−2458.
(35) Bernstein, J. (1992) Effect of crystal environment on molecular structure. In *Accurate Molecular Structures* (Domenicano, A., and Hargittai, I., Eds.) pp 469−497, Oxford University Press.

TX950168B